RSC Advances

PAPER

View Article Online
View Journal | View Issue

Cite this: *RSC Adv.*, 2023, **13**, 3394

A new fluorescent probe for sensing Al^{3+} ions in the solution phase and CH_3COO^- in the solid state with aggregation induced emission (AIE) activity†

Rahul Bhowmick, Payel Mondal and Pabitra Chattopadhyay *

An AIE (aggregation induced emission) active probe **DFP–AMQ** was designed and synthesized as a hexa-coordinated N_2O donor chelator for the selective sensing of Al^{3+} colorimetrically as well as fluorimetrically with a 27-fold fluorescence enhancement for CH_3CN–H_2O (9 : 1, v/v, pH 7.2, HEPES buffer). The fluorescence enhancement occurred through the blocking of ESIPT, chelation enhanced fluorescence effect (CHEF) arose, and as a result fluorescence enhancement was observed through 1 : 1 complexation with Al^{3+} ions. Detailed spectroscopic studies including UV-Vis, FTIR, ^1H NMR, and HRMS studies were carried out to characterize the probable structure of **DFP–AMQ** including the complexation of **DFP–AMQ** with Al^{3+} ions. The spectrophotometric and spectrofluorimetric titrations revealed strong binding towards Al^{3+} and the K_d values were obtained from UV-Vis (3.26×10^{-5} M^{-1}) and fluorescence titration (2.02×10^{-5} M^{-1}). The limit of detection of Al^{3+} by **DFP–AMQ** was 1.11 μM. The quantum yields of **DFP–AMQ** and [**DFP–AMQ**–Al]$^+$ were calculated to be 0.008 and 0.211, respectively. Dynamic light scattering (DLS) studies showed that the sizes of the particles increased with increasing water percentage due to aggregation. SEM (scanning electron microscopy) studies revealed interesting morphological changes in microstructures in which **DFP–AMQ** demonstrated a rod-like shape, which was converted to a spherical-like shape in the presence of Al^{3+} and when **DFP–AMQ** aggregated in H_2O it showed aggregated block-like shape. In the solid phase, **DFP–AMQ** with nitrate has no particular shape, but in the presence of acetate, it converts to stone-like shape. This probe (**DFP–AMQ**) could be employed for on-site Al^{3+} ion detection in the solid state.

Received 3rd November 2022
Accepted 26th December 2022

DOI: 10.1039/d2ra06978d

rsc.li/rsc-advances

1. Introduction

Currently, for the detection of very low levels of molecules/ions, the development of fluorescent sensors has great importance, and in the appraisement of targetable species over fluorescent sensors in solution or in the solid state, several photophysical processes such as CHEF, PET, FRET, and ICT have been considered enormously.[1–5] Many chemosensors present in the solution state compared to the fluorescent materials in solid states have been reported in the literature. Furthermore in the development of chemical as well as biological sensors due to wide-ranging applications, solid-state fluorescent materials have generated extensive interest ranging from the biomedical to optoelectronic fields in almost all phases of human life.[6–10] Aggregation induced emission (AIE), used for the development of efficient fluorescent materials in the solid state is a distinctive photophysical phenomenon, which was first observed in the year 2001 in luminogen aggregation, demonstrating intense emission.[11–13] Furthermore, for the development of fluorescent materials, aggregation induced emission (AIE) has opened a new area. Organic photo-luminescent probes show high fluorescence emissions through aggregation induced emission (AIE) such that the resulting material can bind with molecules *via* strong interaction. The AIE phenomenon occurs from the non-radiative decay when the aggregate state blocks through the control of intra-molecular motions. Likewise, the π–π interactions are prevented by the non-planar conformations, and AIE molecules are fixed when incorporated into solid matrixes, demonstrating strong emission. These special applications make AIE a good candidate for constructing fluorescent materials.[14–17] In dilute solutions, AIE-active sensors show very weak emission and with gradually increasing water percentage, their emission increases because of constrained vibration and rotation.

Aluminium (Al) is the 3rd most abundant element, which plays crucial roles in extensive range of applications including cooking utensils, cosmetics, and potable water supplies.[18,19] Al^{3+} come into the body through the ecosystem and associate with increased incidences that could be responsible for neurotoxicity causing Alzheimer's and Parkinson's diseases, gastrointestinal and colic problems, bone deformation, anaemia, interruption

Department of Chemistry, The University of Burdwan, Golapbag, Burdwan-713104, West Bengal, India. E-mail: pabitracc@yahoo.com

† Electronic supplementary information (ESI) available. See DOI: https://doi.org/10.1039/d2ra06978d

in reproduction, and lung and breast cancer; furthermore, to some extent, certain amount of aluminium is also deadly to plants, fishes, and other living species.[20–24] As such, for these reasons, there is a social as well as biological significance of Al^{3+} ions, and it is very much important to monitor trace levels of Al^{3+} ions. But it is very difficult to find a technique to sense the aluminium ions as it is not in coloured form. Hence, special attention is necessary to develop a chemosensor for aluminium, though strong hydration of Al^{3+} ions with interfering ions and weak coordination is problematic behaviour. Considering these facts, there are several fluorescent sensors for Al^{3+} ions in the solution state based on different photophysical processes.[25–30] However, there are very few probes for the detection of Al^{3+} ions based on the AIE effect.[31,32]

Here we report diformyl phenol and quinoline-based probe **DFP–AMQ**, which is a fluorescent sensor selective on Al^{3+} in the organo-aqueous medium (9 : 1, $CH_3CN : H_2O$, v/v, in HEPES buffer). Through blocking of ESIPT, chelation-enhanced fluorescence effect (CHEF) occurs and as a result, the fluorescence enhancement was observed. Aggregation induced emission enhancement (AIEE) is active in the presence of water. Dynamic light scattering (DLS) studies show the sizes of the particles, which increase with increasing water percentage due to aggregation. In the solid phase, **DFP–AMQ** shows strong fluorescence but in the presence of nitrate anion, fluorescence emission decreases and again fluorescence emission increased selectively under the presence of acetate anions. Scanning electron microscopy (SEM) shows different microstructures in different conditions. Fluorescence microscope images show the different morphologies in different water percentages.

2. Experimental section

2.1 Materials and methods

The initial materials such as 2,6-diformyl phenol (**DFP**, prepared in the laboratory), 6-amino-2-methyl quinoline (**AMQ**) (Sigma Aldrich), were used to develop the ligand **DFP–AMQ** and to prepare Al^{3+} complexes, $Al(NO_3)_3 \cdot 9H_2O$ (Merck, India) was used. Solvents such as CH_3CN, CH_3OH, and dimethyl formamide (DMF) (Merck, India) were of the reagent grade.

2.2 Physical measurements

PerkinElmer 240 elemental analyzer was used for elemental analysis. Infrared spectra (400–4000 cm^{-1}) were recorded using KBr pellets on a Nicolet Magna IR 750 series-II FTIR spectrophotometer. A Bruker 300 MHz NMR spectrometer was used for ^{1}H-NMR recorded in the DMSO-d_6 solvent and using tetramethylsilane ($\delta = 0$) as an internal standard. An Agilent diode-array spectrophotometer (model, Agilent 8453) was used for recording UV-Vis spectra, a Hitachi-7000 spectrofluorimeter was used for recording steady-state fluorescence, ESI-MS^+ (m/z) of the ligand and Al(III)-complex were recorded on a Waters' HRMS spectrometer (model: XEVOG2 QTOF). To analyse the morphology of **DFP–AMQ** in the solid state, FESEM images were taken using an EVO LS10 scanning electron microscope (SEM). For the pH study, a systronics digital pH meter (model 335) was used and 50 mM HCl or NaOH solution was used for the adjustment of pH. The particle size distribution was measured by dynamic light scattering (DLS) on a Malvern Zetasizer Nano ZS90 instrument. Optical fluorescence microscopy images were taken using a LEICA DM1000 LED upright microscope.

2.3 Preparation of DFP–AMQ

2,6-Diformyl phenol (**DFP**) was prepared by following a literature procedure.[33] 2,6-Diformyl-phenol (**DFP**) (0.82 g, 5 mmol) was dissolved in 15 ml EtOH. To this solution, 6-amino-2-methylquinoline (1.58 g, 10 mmol) was added and the solution was refluxed for 5 h. After that, the reaction mixture was filtered and the filtrate was kept at room temperature. After 2 days a red colour crystalline product was formed (yield, 85.57%). ^{1}H-NMR (in DMSO-d_6) (δ, ppm): 2.50 (s, 3H, methyl), 2.66 (s, 6H, methyl), 7.44 (s, 2H, aromatic), 7.80 (m, 2H, aromatic), 7.84 (m, 4H, aromatic), 7.99 (d, 2H, aromatic), 8.24 (d, 2H, aromatic), 14.21 (s, 1H, OH) (please see Fig. S1†). ESI-MS^+ (m/z): 445.26 (**DFP–AMQ** + H^+) [Fig. S2†]. FTIR: 1626 cm^{-1} (CH=N) [Fig. S3†]. Melting point: 98 ± 1 °C. Elemental analysis: expected: C, 78.36%; H, 5.44%; N, 12.60%; calculated: C, 78.31%; H, 5.37%; N, 12.52%.

2.4 Synthesis of [DFP–AMQ–Al]$^+$

DFP–AMQ (0.444 g, 1 mmol, was dissolved in a few drops of DMF), then, 25 ml CH_3CN was added to $Al(NO_3)_3 \cdot 9H_2O$ (0.375 g, 1 mmol in 5 ml MeOH solution) dropwise with continuous stirring. After 1.5 hours, the solution was filtered off and the filtrate was kept aside undisturbed. After one day, [(**DFP–AMQ**)Al)]$^+$ was crystallised. It was collected by filtration, washed several times with MeCN, and dried in air. Several trials to grow single crystals failed. ^{1}H-NMR (in DMSO-d_6) (δ, ppm): 2.50 (s, 3H, methyl), 2.67 (s, 3H, methyl), 2.83 (s, 3H, methyl), 7.48–8.30 (12H, aromatic), 9.10 (s, 1H, CH=N), 9.20 (s, 1H, CH=N) (Fig. S4†). ESI-MS^+ (m/z): 568.52[Al(**DFP–AMQ**)$(H_2O)_2]^+$, 596.55 [Al(**DFP–AMQ**)$(CH_3OH)_2]^+$ (Fig. S5†). FTIR: 1613 cm^{-1} (CH=N) [Fig. S6†].

2.5 Solution preparation for UV-Vis and fluorescence studies

A stock solution of **DFP–AMQ** was prepared (1.0×10^{-3} M) by dissolving the **DFP–AMQ** in 10 ml CH_3CN for both UV-visible and fluorescence emission titrations. Similarly, another stock solution of Al^{3+}, 1.0×10^{-3} M was prepared in de-ionised water. 10 mM HEPES buffer (9 : 1 $CH_3CN : H_2O$) was prepared and the solution of pH was adjusted to 7.2 by using HCl and NaOH. 2.5 ml of the prepared buffer solution was pipetted out into a 5 ml cuvette to which 20 μM of the probe was added and Al^{3+} ion was added gradually starting from 0 to 30 μM in a regular interval of volume and UV-visible and fluorescence emission spectra were recorded for each solution. Path lengths of the cells used for absorption and emission studies were 1 cm. Fluorescence measurements were performed using a 5 nm × 5 nm slit width.

2.6 Job's study

Changing molar concentrations of two reactants Job's study was performed but their sum remains constant. The fluorescence emission of each solution is measured at a suitable wavelength and plotted against the mole fraction of one reactant. A maximum in fluorescence emission occurs at the mole ratio corresponding to the combined ratio of the reactants (Fig. S7†).

2.7 Time-correlated single photon counting measurements

Time-correlated single photon counting (TCSPC) measurements were performed in pure acetonitrile and in 10 mM HEPES buffer (9 : 1 $CH_3CN : H_2O$) of pH 7.2. The fluorescence decay rates of **DFP–AMQ** and the [**DFP–AMQ**–Al]+ complex were measured at 25 °C. TCSPC was performed by photoexcitation at 400 nm using a Hamamatsu MCP photomultiplier (R3809). The resulting data were analyzed by using the following equation with the help of the IBH DAS6 software.

$$F(t) = \sum_i a_i \exp\left(-\frac{t}{\tau}\right)$$

where a_i represents the ith pre-exponential factor and t is the decay time.

3. Results and discussion

3.1 Synthesis and characterization

2,6-Diformyl-phenol (**DFP**, **1**)–6-amino-2methylquinoline (**AMQ**, **2**) based (**DFP–AMQ**) was produced by a Schiff base condensation in the ethanolic medium, which showed reddish colour, as shown in Scheme 1. This ligand has N_2O donor atoms which are potentially hexa-coordinated binding to one metal ion leading to the formation of a mononuclear complex. The **DFP–AMQ** ligand and its Al^{3+} complex were isolated and characterized using various physicochemical (NMR, IR, and ESI-MS^+ (m/z)) (Fig. S1–S6†) methods.

3.2 UV-Vis absorption studies

The ESIPT phenomena are often exhibited by intramolecular hydrogen-bonded organic chromophores. In the route of ESIPT, which is an intramolecular form of photo acids and photo bases in chemistry where the molecule environs acidic as well as basic groups; upon excitation, the migration of acidic proton to the basic site occurs. Mostly, ESIPT processes are assisted by either five-or six-membered intramolecular hydrogen bonds in the ground state and commonly require a very minute movement of nuclei. The solvent is not required in intrinsic ESIPT to mediate such a proton transfer process and is barrierless in non-polar solvents occurring in the sub-picoseconds time region.[34] In methyl salicylate, the first reported ESIPT reaction was observed.[35] The UV-visible absorption spectral properties of **DFP–AMQ** were measured in 9 : 1 CH_3CN–H_2O at pH 7.2 HEPES buffer. The UV-visible absorption spectrum of **DFP–AMQ** showed two important transitions with strong absorbance at 333 and 369 nm. As per Scheme 2, due to ESIPT the enol and keto tautomers of **DFP–AMQ** are in equilibrium. At 369 nm, the band is assigned to the transition to keto (quinoid) form. The absorption bands of **DFP–AMQ** at 369 and 333 nm decrease gradually upon the gradual addition of Al^{3+}; however, two new peaks appeared at 432 and 486 nm, thereby, the formation of one isosbestic point at 400 nm, which clearly designates a clean transformation of the free ligand to its metal-bound state (Fig. 1).

This indicates the chelation of Al^{3+} by the hexadentate ligand moiety giving [Al(**DFP–AMQ**)]$^+$. The spectral change (decrease in

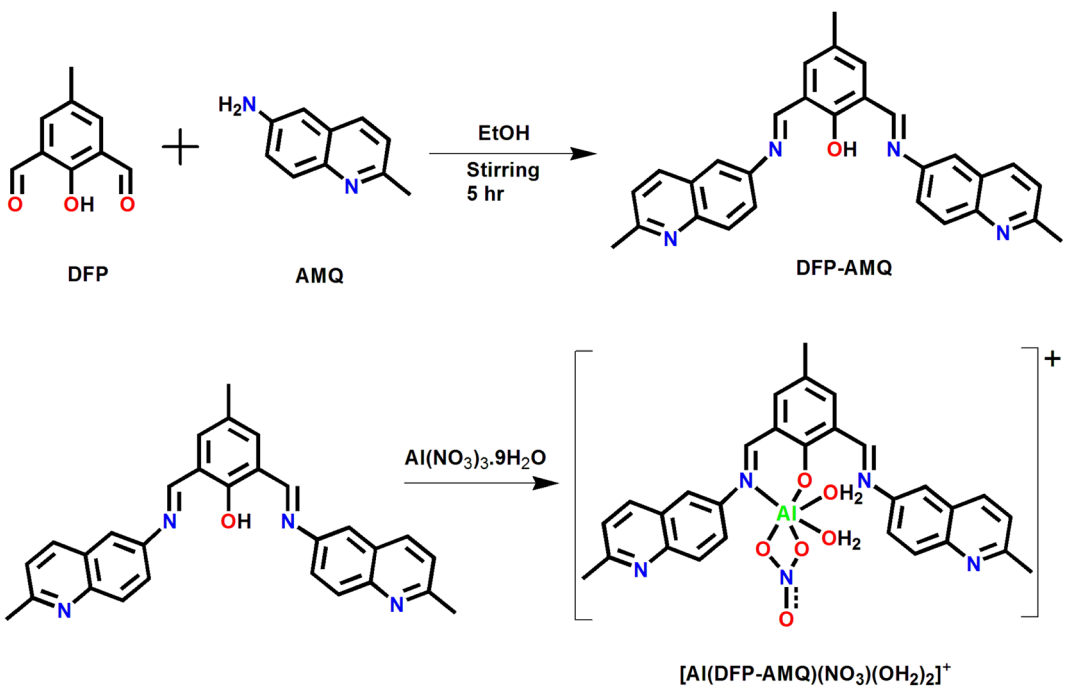

Scheme 1 The synthetic route of DFP–AMQ.

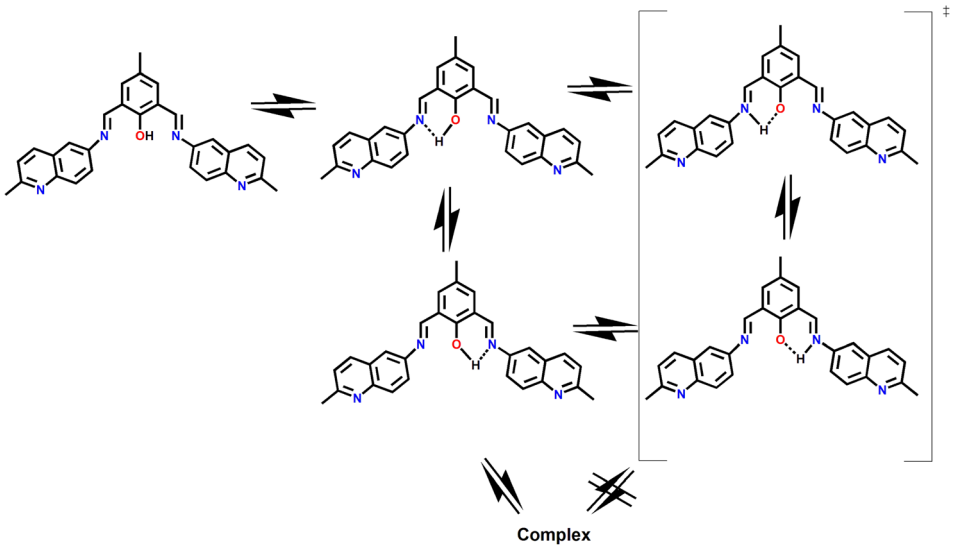

Scheme 2 The probable pathway for ESIPT.

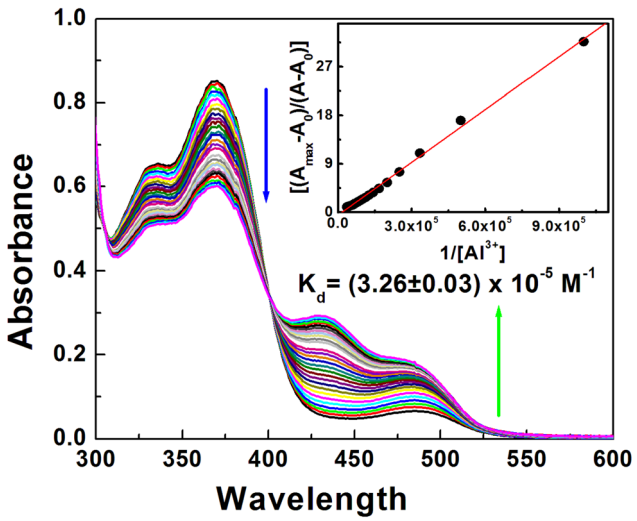

Fig. 1 Absorption titration of **DFP–AMQ** (20 μM) with Al^{3+} (0–30 μM) in CH_3CN–H_2O (9 : 1, v/v, pH 7.20, 10 mM HEPES buffer). Inset shows Benesi–Hildebrand fitting of the data.

absorption spectra at 369 nm and increase at 432 and 486 nm) obviously indicates that the addition of Al^{3+} ions induces the decrease in the concentration of free ligands both in keto and enol forms. Here, the nitrogen atom takes part in the coordination with Al^{3+} and the formation of the complex inhibits the ESIPT (Scheme 2). UV-Vis absorption studies were performed to investigate the cation binding affinities towards aluminium ions, and when a change in the absorbance at 432 and 486 nm was plotted against $[Al^{3+}]$, with increasing $[Al^{3+}]$ a gradual increase in the absorbance was observed.

A linear form of the Benesi–Hildebrand equation (eqn (1)) was used to obtain the dissociation constant and stoichiometry of the complexation, where, A_0 and A_{max} are the absorbances of the ligand in the absence and in the presence of excess metal ions, respectively, and n is the stoichiometry (**DFP–AMQ** : Al^{3+}) of the reaction. A linear least square-fit of $(A_{max} - A_0)/(A - A_0)$ against 1/[M] clearly demonstrates a 1 : 1 stoichiometry of the reaction ($n = 1$), which also gives an apparent dissociation constants $K_d = (3.26 \pm 0.03) \times 10^{-5}$ M.

$$\frac{A_{max} - A}{A - A_0} = 1 + \frac{1}{K_d[M]^n} \quad (1)$$

3.3 Fluorescence emission studies

The fluorescence emission spectra of **DFP–AMQ** and its titration with Al^{3+} were recorded in CH_3CN–H_2O (9 : 1, v/v, pH 7.20, HEPES buffer) (Fig. 2) at $\lambda_{ex} = 400$ nm. The binding between the

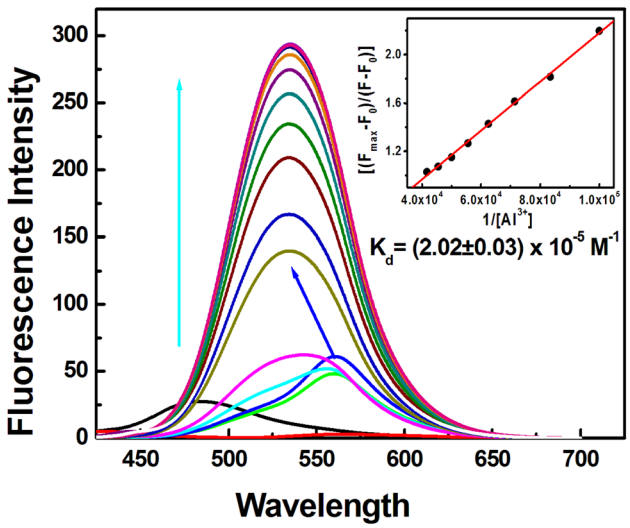

Fig. 2 Fluorescence titration of **DFP–AMQ** (20 μM) with Al^{3+} (0–30 μM) in CH_3CN–H_2O (9 : 1, v/v, pH 7.20, 10 mM HEPES buffer), λ_{ex} = 400 nm. Inset shows Benesi–Hildebrand fitting of the data.

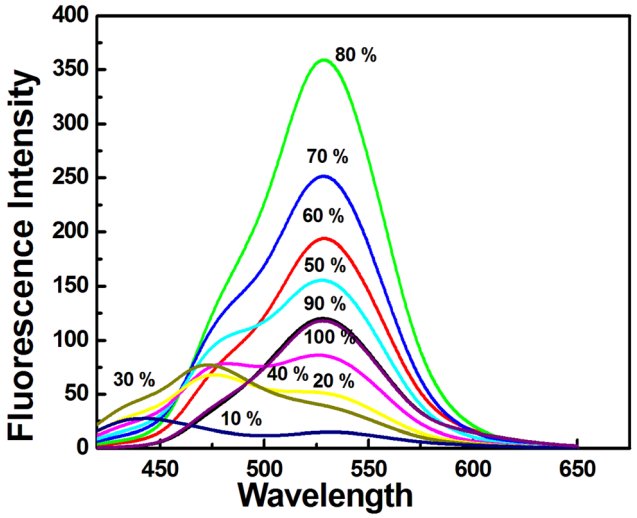

Fig. 3 Fluorescence emission of **DFP–AMQ** with different percentages of H_2O, $\lambda_{ex} = 400$ nm.

free **DFP–AMQ** and Al^{3+} leads to the chelation-enhanced fluorescence (CHEF) effect causing ~27-fold enhancement due to the increased structural rigidity of the formed complexes (Fig. 2). Upon excitation at 400 nm, the isosbestic point in the absorption spectra, in the beginning, there is a gradual increase in the fluorescence intensity (FI) at $\lambda_{em} = 561$ nm, then a blue shift occurs to $\lambda_{em} = 535$ nm with the increase in $[Al^{3+}]$ (Fig. 2). This shifting occurs due to the intramolecular charge transfer (ICT).[36]

To analyse the binding constant from the fluorescence titration data, a linear form of the Benesi–Hildebrand equation (eqn (1)) was used, which gives the apparent dissociation constant $K_d = (20.2 \pm 0.03) \times 10^{-5}$ M. The binding constants value obtained from UV-Vis and the fluorescence titration data clearly indicate the agreement between two K_d values.

3.4 Selectivity study

The selectivity study showed that the probe could selectively detect Al^{3+} ions, which were not disturbed by other metal ions such as biologically rich K^+, Na^+, Mg^{2+}, and Ca^{2+} metal ions, various transition metal ions, namely Fe^{2+}, Fe^{3+}, Mn^{2+}, Ni^{2+}, Cr^{3+}, Co^{2+}, and Cu^{2+}, and heavy metal ions such as Hg^{2+}, Cd^{2+}, Zn^{2+}, and Pb^{2+}, and there was no interference (Fig. S8†). The fluorescent chemosensor was found to bind Al^{3+} reversibly when it reacted with excess EDTA (Fig. S9†). Moreover, no major change in the emission spectra was found even on excess addition of the above-mentioned interfering metal ions (Fig. S8†).

3.5 Calculation of LOD

To determine the detection limit, fluorescence titration of **DFP–AMQ** with Al^{3+} was carried out by adding a micromolar concentration of Al^{3+} in **DFP–AMQ** (20 μM) and by the 3σ method. The LOD was calculated as follows:

$$\mathrm{LOD} = 3 \times S_d/S$$

where, S_d is the standard deviation of the intercept of the blank (**DFP–AMQ** only) obtained from a plot of fluorescence intensity (FI) *vs.* [**DFP–AMQ**], and S is the slope obtained from the linear part of the plot of FI *vs.* $[Al^{3+}]$. Using the 3σ method calculation, the detection limit (LOD) of Al^{3+} was 1.11 μM (Fig. S10†).

3.6 pH study

For real applications, the appropriate pH conditions required for the successful action of the sensor were estimated. The probe **DFP–AMQ** showed very weak fluorescence emission between pH 2 and 8, while the **DFP–AMQ**–Al complex showed very strong fluorescence emission between pH 5 and 8 in 10 mM HEPES buffer, clearly indicating that this pH range is suitable for fluorescence studies for the complexation with Al^{3+} (Fig. S11†). The fluorescence emission of free **DFP–AMQ** increases beyond pH 10.0 due to the acid dissociation of the proton.

3.7 Aggregation induced emission (AIE) of DFP–AMQ

AIE was observed when the percentage of water was varied. Here, CH_3CN and H_2O were used as good and poor solvents,

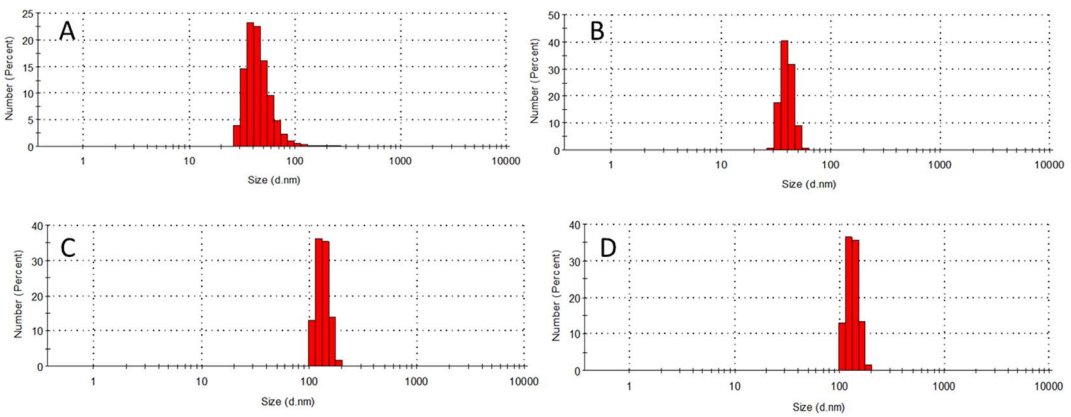

Fig. 4 Dynamic light scattering (DLS) study of **DFP–AMQ** with different percentages of H_2O: (A) 0%, (B) 20%, (C) 50%, and (D) 80% and shows the sizes (A) 40.48 nm, (B) 44.77 nm, (C) 142.8 nm and (D) 154.62 nm.

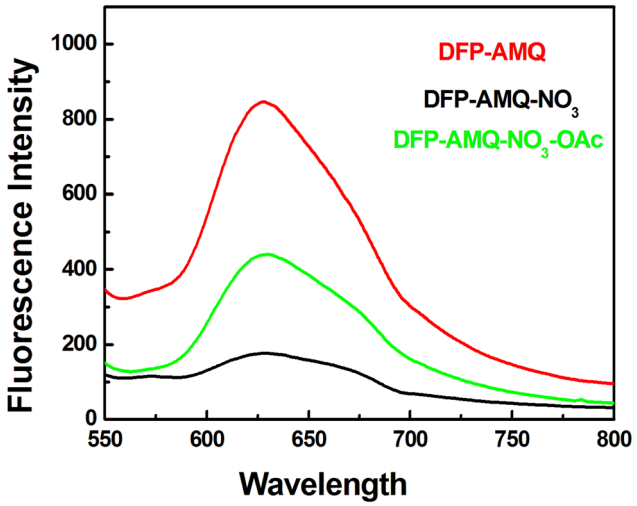

Fig. 5 Fluorescence emission of **DFP–AMQ** with NO_3^- and both NO_3^-–OAc^- in the solid state (at $\lambda_{ex} = 450$ nm).

respectively. This study revealed that with increasing water percentages (0–100) the fluorescence emission increases towards the red region and at 80% of water content, it showed a maximum emission at 528 nm (Fig. 3). This observation clearly indicates the J-type aggregation induced emission due to the presence of a large π-conjugated planar structure. In the aggregates, however, **DFP–AMQ** molecules face strong face-to-face π–π interactions between two **DFP–AMQ** molecules, and these are expressed directly by the overlaps in π-conjugated systems. In CH_3CN medium **DFP–AMQ** showed a typical AIE phenomenon having very weak fluorescence.

Upon increasing the volume of water percentages up to 80%, fluorescence emission enhancement occurred due to the emissive TICT state (quasi-TICT*). Upon further increase of water from 80 to 99 in vol%, the fluorescence emission intensity decreased, which is known. Due to the restriction of intramolecular motion (RIM) in the aggregated state ACQ effect occurs. Consequently, the formation of a planar structure from the twisted structure in the excited state is accountable for the solution state quenching.

3.8 DLS measurements

To realise the aggregation behaviour of **DFP–AMQ**, dynamic light scattering (DLS) experiments were performed in the presence of varying water percentages (Fig. 4). DLS studies revealed that the average size of the aggregated **DFP–AMQ** in CH_3CN/H_2O ($f_w = 10\%$) was *ca.* 40.48 nm, as shown in Fig. 4A. This also signifies that **DFP–AMQ** can be well-dissolved and dispersed in CH_3CN/H_2O solution. However, an increase in the volume of the water percentage (up to 80%) led to a significant increase in the average size of aggregates (Fig. 4D), which also supported the observed AIE activity of the probe **DFP–AMQ**. While, the average size of the aggregates became 154.62 nm in 80% volume

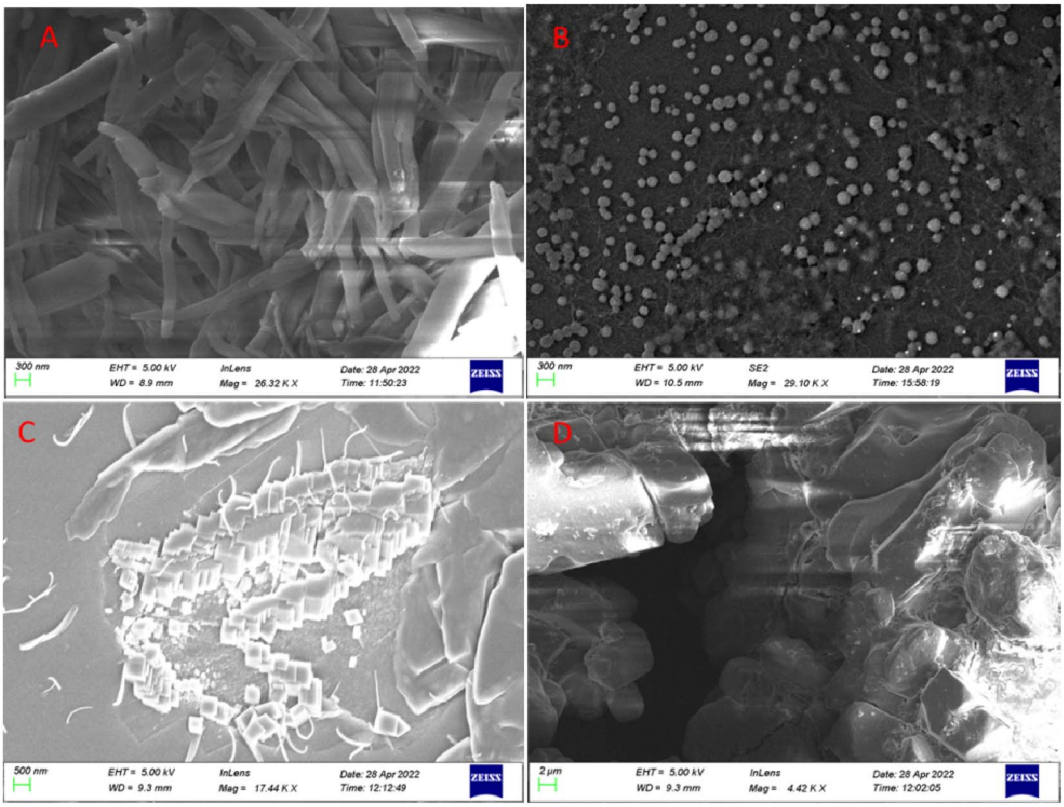

Fig. 6 SEM images of (A) **DFP–AMQ** (solid sample), (B) [**DFP–AMQ**–Al]$^+$ (solid sample), (C) **DFP–AMQ** in the presence of H_2O, (D) **DFP–AMQ**–nitrate–acetate.

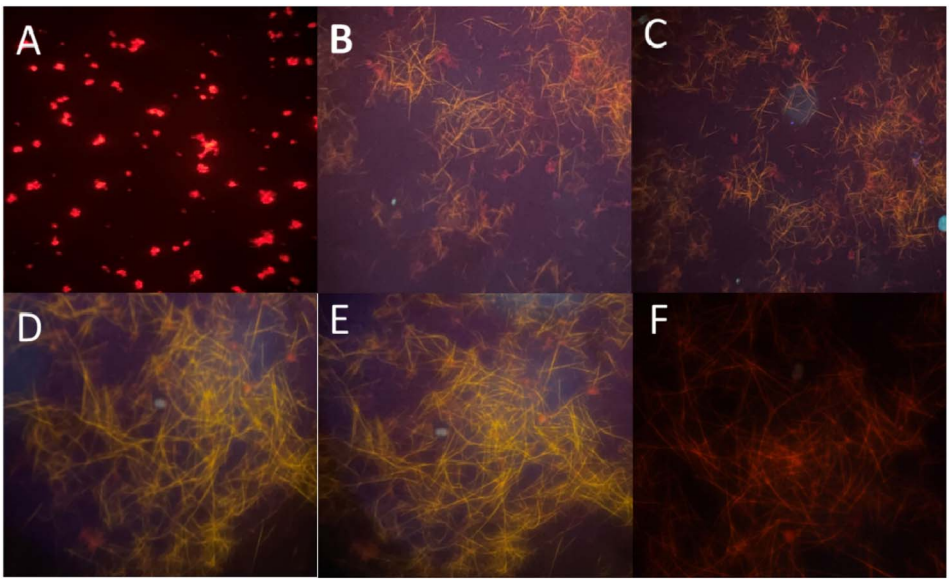

Fig. 7 Fluorescence microscope images of (A) **DFP–AMQ**, **DFP–AMQ** in the presence of (B) 20% H_2O, (C) 50% H_2O, (D) 70% H_2O, (E) 80% H_2O and (F) 100% H_2O.

percentage of water (Fig. 4D), which is in good agreement with the spectroscopic studies.

Now to prove the aggregation behavior of **DFP–AMQ** in the presence of Al^{3+} ions, we also carried out the DLS measurements in the presence of 0%, 20%, and 50% water. However, an increase in the volume of water percentage led to a significant increase in the average size of aggregates (Fig. S12†), which also supported the observed AIE activity of the probe **DFP–AMQ** in the presence of Al^{3+}. The average sizes of the above solutions are 204.04 nm, 297.41 nm, and 315.27 nm, respectively.

3.9 Solid state emission

The solid-state emission spectra of **DFP–AMQ** were measured at $\lambda_{ex} = 450$ nm and its fluorescence intensity (FI) was found at $\lambda_{em} = 628$ nm. **DFP–AMQ** showed fluorescence emission due to the aggregation, which is clearly indicated by the scanning electron microscope studies. When the solid **DFP–AMQ** was ground in a mortar pastel with solid sodium nitrate, the emission decreased and after that, this material was ground with solid sodium acetate, and again the emission spectra were observed with very high intensity, almost double that of the solid **DFP–AMQ**–NO_3. We also recorded the emission spectra with other anion salts, but only the acetate ion responded (Fig. S13†). Hence, this study revealed that in the solid state after grinding with sodium nitrate, it recognized only acetate ions (Fig. 5).

3.10 SEM study

The morphologies of **DFP–AMQ**, its Al-complex, **DFP–AMQ** in 80% water, and **DFP–AMQ** with nitrate and **DFP–AMQ**–nitrate–acetate were studied using the scanning electron microscopy (SEM) analysis, which provided the evidence for the changes in the morphology of **DFP–AMQ** (rod-like shape) to **DFP–AMQ**–Al (spherical-like shape) aggregate formation of **DFP–AMQ**–H_2O (aggregated-block-like shape), **DFP–AMQ** with nitrate (no particular shape) and **DFP–AMQ**–nitrate–acetate (stone-like shape) (Fig. 6).

3.11 Fluorescence microscope imaging

Fluorescence microscope images show that the solid **DFP–AMQ** showed fluorescent images after treatment with different percentages of water in the solution state and after drop casting on the slide, needle-like aggregated shapes were found (Fig. 7).

3.12 Time-correlated single photon counting measurements

Time-correlated single-photon counting measurements for the lifetime experiments for the **DFP–AMQ** in CH_3CN and CH_3CN–H_2O and **DFP–AMQ**–Al^{3+} were performed. For the pure CH_3CN, the lifetime of **DFP–AMQ** was 0.09 nS but in the organic aqueous medium, the lifetime increased to 4.59 nS due to its aggregation behavior, while the complex showed a lifetime of 9.58 nS (Fig. S14†).

4. Conclusion

In summary, we have successfully designed and synthesized a **DFP–AMQ**-based hexa-coordinating N_2O donor ligand that selectively recognizes Al^{3+} colorimetrically and fluorimetrically with ~27-fold fluorescence enhancement in the presence of a number of various interfering metal ions, and it was found to undergo 1 : 1 complexation in MeCN–H_2O (9 : 1, v/v, pH 7.2, HEPES buffer). By blocking ESIPT, chelation-enhanced fluorescence effect (CHEF) arose and the resulting fluorescence enhancement was observed. The complexation of **DFP–AMQ** to Al^{3+} was confirmed by ^1H NMR and HRMS studies. The K_d values measured were 3.26×10^{-5} M^{-1} and 2.02×10^{-5} M^{-1}

obtained from the UV-Vis and fluorescence titrations, respectively, revealing the strong binding towards Al^{3+} ions. The limit of detection of Al^{3+} by **DFP–AMQ** was 1.11 μM. The quantum yields of the **DFP–AMQ** and [**DFP–AMQ**–Al]$^{+}$ were 0.008 and 0.211, respectively. Dynamic light scattering (DLS) studies showed an increase in the sizes of the particles with increasing water percentage and this was due to aggregation. Under the different reaction conditions, SEM studies revealed interesting microstructures. The rod-like shape of **DFP–AMQ** was converted to a spherical-like shape in the presence of Al^{3+} ions, whereas the block-like shape of the aggregated **DFP–AMQ** occurring in H_2O was observed. In the solid phase, **DFP–AMQ** with nitrate had no particular shape, but in the presence of acetate, it was converted to a stone-like shape. The observed results indicate that this probe (**DFP–AMQ**) is very much useful for on-site Al^{3+} ions detection in the solid state through a fast, simple, and eco-friendly process; it may be useful in OLED and to develop biomedicine for Alzheimer's and Parkinson's diseases.

Conflicts of interest

The authors declare no conflicts of interest.

Acknowledgements

Rahul Bhowmick gratefully acknowledges UGC New Delhi, India for Dr D. S. Kothari Postdoctoral Fellowship (award letter no. F.4-2/2006 (BSR)/CH/20-21/0201) and Payel Mondal is grateful to CSIR New Delhi for fellowship (award letter no. 09/0025(11972)/2021-EMR-I).

References

1 K. Dhara, S. Lohar, A. Patra, P. Roy, S. K. Saha, G. C. Sadhukhan and P. Chattopadhyay, *Anal. Chem.*, 2018, **90**, 2933–2938.
2 S. Pal, M. Mukherjee, B. Sen, S. Lohar and P. Chattopadhyay, *RSC Adv.*, 2014, **4**, 21608–21611.
3 S. Pal, S. Lohar, M. Mukherjee, P. Chattopadhyay and K. Dhara, *Chem. Commun.*, 2016, **52**, 13706–13709.
4 Y. Ma, S. Huang, M. Deng and L. Wang, *ACS Appl. Mater. Interfaces*, 2014, **6**, 7790–7796.
5 R. S. Singh, R. K. Gupta, R. P. Paitandi, A. Misra and D. S. Pandey, *New J. Chem.*, 2015, **39**, 2233–2239.
6 C. T. Chen, *Chem. Mater.*, 2004, **16**, 4389–4400.
7 W. Z. Yuan, Y. Gong, S. Chen, X. Y. Shen, J. W. Y. Lam, P. Lu, Y. Lu, Z. Wang, R. Hu, N. Xie, H. S. Kwok, Y. Zhang, J. Z. Sun and B. Z. Tang, *Chem. Mater.*, 2012, **24**, 1518–1528.
8 S. Reineke, F. Lindner, G. Schwartz, N. Seidler, K. Walzer, B. Lussem and K. Leo, *Nature*, 2009, **459**, 234–238.
9 Y. Sun, N. Giebink, C. H. Kanno, B. Ma and M. E. Thompson, *Nature*, 2006, **440**, 908–912.
10 S. Tonzani, *Nature*, 2009, **459**, 312–314.
11 Z. He, C. Ke and B. Z. Tang, *ACS Omega*, 2018, **3**, 3267–3277.
12 M. Shyamal, P. Mazumdar, S. Maity, G. P. Sahoo, G. Salgado-Morán and A. Misra, *J. Phys. Chem. A*, 2016, **120**, 210–220.
13 X. Zhao, C. Ji, L. Ma, Z. Wu, W. Cheng and M. Yin, *ACS Sens.*, 2018, **3**, 2112–2117.
14 Z. Zhao and F. C. Spano, *J. Chem. Phys.*, 2005, **122**, 114701.
15 A. Eisfeld and J. S. Briggs, *Chem. Phys.*, 2006, **324**, 376–384.
16 Y. Hong, J. W. Y. Lam and B. Z. Tang, *Chem. Soc. Rev.*, 2011, **40**, 5361–5388.
17 J. Gierschner, L. Lüer, B. M. Medina, D. Oelkrug and H. J. Egelhaaf, *J. Phys. Chem. Lett.*, 2013, **4**, 2686–2697.
18 P. D. Darbre, F. Mannello and C. Exley, *J. Inorg. Biochem.*, 2013, **128**, 257–261.
19 V. Rondeau, D. Commenges, H. Jacqmin-Gadda and J. F. Dartigues, *Am. J. Epidemiol.*, 2000, **152**, 59–66.
20 S. Pal, B. Sen, M. Mukherjee, M. Patra, S. Lahiri (Ganguly) and P. Chattopadhyay, *RSC Adv.*, 2015, **5**, 72508–72514.
21 E. Alvarez, M. L. F. Marcos, C. Monterroso and M. J. F. Sanjurjo, *For. Ecol. Manage.*, 2005, **211**, 227–239.
22 J. Barcelo and C. Poschenrieder, *Environ. Exp. Bot.*, 2002, **48**, 75–92.
23 T. P. Flaten and M. Odegard, *Food Chem. Toxicol.*, 1988, **26**, 959–960.
24 R. A. Yokel, *Neurotoxicology*, 2000, **21**, 813–828.
25 K. Tiwari, M. Mishra and V. P. Singh, *RSC Adv.*, 2013, **3**, 12124–12132.
26 M. Mukherjee, B. Sen, S. Pal, S. Banerjee, S. Lohar and P. Chattopadhyay, *RSC Adv.*, 2014, **4**, 64014–64020.
27 M. Mukherjee, A. Maji, S. Pal, B. Sen and P. Chattopadhyay, *Spectrochim. Acta, Part A*, 2016, **157**, 11–16.
28 B. Sen, S. Pal, S. Banerjee, S. Lohar and P. Chattopadhyay, *Eur. J. Inorg. Chem.*, 2015, 1383–1389.
29 B. Sen, M. Mukherjee, S. Banerjee, S. Pal and P. Chattopadhyay, *Dalton Trans.*, 2015, **44**, 8708–8717.
30 M. Mukherjee, S. Pal, S. Lohar, B. Sen, S. Sen, S. Banerjee, S. Banerjee and P. Chattopadhyay, *Analyst*, 2014, **139**, 4828–4835.
31 S. Dey, R. Purkait, K. Pal, K. Jana and C. Sinha, *ACS Omega*, 2019, **4**, 8451–8464.
32 M. Shyamal, P. Mazumdar, S. Maity, S. Samanta, G. P. Sahoo and A. Misra, *ACS Sens.*, 2016, **1**, 739–747.
33 R. Bhowmick, R. Alam, T. Mistri, K. K. Das, A. Katarkar, K. Chaudhuri and M. Ali, *RSC Adv.*, 2016, **6**, 11388–11399.
34 S. Scheiner, *J. Phys. Chem. A*, 2000, **104**, 5898–5909.
35 A. Weller, *Zeitschrift für Elektrochemie*, 1956, **60**, 1144–1147.
36 J. Y. Choi, D. Kimb and J. Yoon, *Dyes Pigm.*, 2013, **96**, 176–179.